Validation of Universal Cryogenic Flow Boiling Correlations in Thermal Desktop for Liquid Hydrogen

Erin Tesny[1]
NASA Glenn Research Center, Cleveland, OH, 44135

Brian P. Johnson[2]
Michigan Technological University, Houghton, MI, 49931

Jason Hartwig[3], Mariano Mercado[4],
NASA Glenn Research Center, Cleveland, OH, 44135

Vishwanath Ganesan[5], Issam Mudawar[6]
Purdue University, West Lafayette, IN, 47907

Developing accurate models of two-phase cryogenic flow will reduce risk and reduce margins for future NASA vehicles such as the Nuclear Thermal Propulsion (NTP) system. Currently there is a need for more accurate, direct cryogenic data-anchored models for various boiling and two-phase phenomena. The focus of the current work is on modeling steady state cryogenic flow boiling in the transfer line that connects a propellant storage tank to an engine or customer receiver tank. This paper presents Thermal Desktop model validation results against several historical liquid hydrogen (LH_2) heated tube experiments that cover a wide range of inlet conditions, mass flux, and heat flux. New universal cryogenic flow boiling correlations were recently developed and anchored to the largest cryogenic flow boiling database assembled in the world to-date. The new universal correlations are patched together and implemented into Thermal Desktop to compare model performance against the built-in flow boiling correlations. Axial wall temperature predictions as a function of preponderant parameters like heat flux, mass flux, inlet pressure, inlet quality, tube diameter, etc. using the two sets of flow boiling correlations are compared against the experimental data. Overall, the Thermal Desktop model with the new universal cryogenic flow boiling correlations demonstrates an improvement in predictive performance over the Thermal Desktop model using built-in correlations for both wall temperature and location of critical heat flux compared to the data for LH_2 flow boiling in heated tubes.

Nomenclature

G	=	Mass flux, [kg/m^{2}s]
h_{tp}	=	Two-phase heat transfer coefficient, [W/m^{2}K]
P	=	Pressure, [Pa]
c_p	=	Specific heat at constant pressure, [J/kg.K]

[1]Aerospace Engineer, Fluids and Cryogenics Branch, 21000 Brookpark Road, Cleveland, OH, 44135
[2]Undergraduate Student, Michigan Technological Institute, 1400 Townsend Drive
Houghton, MI 49931
[3]Research Aerospace Engineer, Fluids and Cryogenics Branch, 21000 Brookpark Road, Cleveland, OH, 44135, AIAA Associate Fellow
[4]Aerospace Engineer, Fluids and Cryogenics Branch, 21000 Brookpark Road, Cleveland, OH, 44135
[5]Ph.D. Candidate, Boiling and Two-Phase Flow Laboratory, School of Mechanical Engineering, Mechanical Engineering Building, 585 Purdue Mall, West Lafayette, IN 47907
[6]Betty Ruth and Milton B. Hollander Family Professor of Mechanical Engineering, School of Mechanical Engineering, Mechanical Engineering Building, 585 Purdue Mall, West Lafayette, IN 47907, AIAA Senior Member

CHFF	=	Scaling parameter on CHF estimation
D	=	Inner tube diameter, [m]
E	=	Experiment value
F	=	Two-phase multiplier
G	=	Mass flux, [kg/m^{2}s]
g	=	Gravity, [m/s^2]
HFFL	=	Scaling parameter on Leidenfrost temperature estimation
h_{fg}	=	Heat of vaporization, [J/kg]
k	=	Thermal conductivity, [W/m*K]
L	=	Length, [m]
L_h	=	Hydraulic length, [m]
M	=	Modeling value
QTIE	=	Heat rate through tie, [W]
q''	=	Heat flux, [W/m^2]
P	=	Pressure, [kPa]
Pr	=	Prandtl number
Re	=	Reynolds number
S	=	Nucleate boiling suppression factor
T	=	Temperature, [K]
TEF	=	Effective fluid temperature, [K]
U	=	Heat transfer coefficient, [W/m^{2}K]
UA	=	Heat transfer conductance, [W/K]
UAM	=	Scaling multiplier
X	=	Quality
XNB	=	Cutoff value for nucleate boiling
$x_{e,in}$	=	Inlet thermodynamic equilibrium quality based on pressure at inlet of heated length
Y	=	Heat transfer correction factor
z	=	Axial location, [m]
z_{CHF}	=	Axial location at the point of critical heat flux, [m]

Greek Symbols

α	=	Thermal diffusivity, [m^2/s]
ρ	=	Density, [kg/m^3]
σ	=	Surface tension, [N/m]
φ	=	Blending coefficient

Subscripts

CHF	=	Critical Heat Flux
dfb	=	Departure from nucleate boiling
FB	=	Film boiling
g	=	Gas
In	=	Inlet
l	=	liquid
leid	=	Leidenfrost point
mac	=	Macro-convective heat transfer coefficient
mic	=	Micro-convective heat transfer coefficient
min-FB	=	Minimum
pre-CHF	=	*A*xial locations before z_{CHF}
post-CHF	=	Axial locations after z_{CHF}
tie	=	Tie
tp	=	Two-phase
v	=	Vapor

I. Introduction

Future in-space cryogenic propellant transfer architectures are a necessary component for facilitating future NASA and other aerospace missions on a large scale. The aerospace community's goals of establishing sustained crewed presences on the Moon and Mars will require ascent and descent stages, cryogenic fuel depots, and next generation propulsion systems such as nuclear thermal propulsion (NTP) or nuclear electric/chemical systems [1]. Cryogenic systems offer unique benefits in efficiency and specific impulse, at launch mass savings, as well as safety and environmental benefits as compared to toxic non-cryogenic propellants.

While using cryogenic propellants does offer many benefits, cryogens also present a unique set of challenges. Liquid cryogens only exist at exceptionally low temperatures; due to this, high heat transfer rates, and flow boiling are certainties in the cryogenic propellant transfer process. For most use cases of cryogens, single phase liquid flow is highly desired or is a requirement, because having vapor present in the flow may damage pumps and valves or reduce engine performance. Before single-phase cryogenic propellant can be transferred, the connecting transfer line and associated hardware must be chilled down to cryogenic saturation temperatures. Chilldown is usually performed in a cyclic pattern so that the system can chill-in and allow cold liquid to displace the boil-off gas. For steady state transfer line operation, the subcooled margin of the liquid in the propellant storage tank must be sufficiently high to overcome the parasitic heat leak into the transfer line such that single-phase liquid is achievable at the exit of the line. In order to determine the required insulation thickness or achievable operating ranges, high accuracy models of the steady state flow boiling process must be developed and validated.

The success of these future in-space cryogenic propellant transfer systems and missions may be augmented by accurately being able to model the various stages of cryogenic transfer and storage. Poor models lead to higher launch mass due to the need for conservative assumptions and safety factors. Nearly all computational fluid dynamics (CFD) models as well as lumped capacitance or "nodal" codes, such as Thermal Desktop (TD), rely on robust models, correlations, and subroutines at the fundamental level. Recently, attention has been drawn to the fact that existing room-temperature based models and correlations do a poor job in predicting certain cryogenic flow phenomena, yet most correlations used in the most popular thermal/fluid design codes are based on room-temperature fluids, and thus severely over- or underpredict cryogenic flow boiling heat transfer coefficients [2, 3]. For steady state or heated tube configurations, the disparity between these models and cryogenic data is as high as 400%. To address this concern, direct cryogenic data-anchored correlations and subroutines are systematically being developed and validated for multiple cryogenic propellants and transfer phenomena across the board.

This paper presents the implementation of recently developed universal correlations for saturated flow boiling heat transfer coefficients (HTC) and critical heat flux (CHF) [4-7] into Thermal Desktop and presents a comparison in performance between the default correlations built-in to Thermal Desktop against the universal correlations at modeling historical liquid hydrogen (LH_2) data sets from Hendricks et al. [8] and Lewis et al. [9]. This paper will first give a background to the boiling curve and different boiling regimes, followed by the motivation for developing the universal correlations. Then a description of the Thermal Desktop models used for comparing the universal correlations and built-in correlations is given, as well as a description of the implementation of the universal correlations into Thermal Desktop. Finally, results are compared between the different model runs. Appendix A presents the tabulated error values for individual cases from [8, 9].

A. The Boiling Curve

The boiling curve shown in Figure 1 describes the relationship between wall superheat (difference between tube wall and bulk fluid saturation temperature) and heat flux. The boiling curve applies for the boiling heat transfer of any fluid. Tracing the boiling curve from left to right (red line) gives the heating configuration, or steady state boiling configuration. In the heating configuration, the fluid starts as pure single-phase liquid which is heated by an external source until the onset of nucleate boiling (ONB) occurs. Once ONB is reached, small, isolated bubbles continue to form on the heated surface, where they continually depart from the surface and are replenished with fresh liquid, creating considerable mixing near the surface which generates high HTCs and thus allows for high surface heat flux. As the heat flux increases further, the isolated vapor bubbles from nucleate boiling turn into vapor jets and columns, reducing the wall-to-fluid HTC and eventually leading to CHF. Once CHF is reached, a minute increase in heat flux results in a rapid unsteady rise in wall temperature and thus wall superheat. Post-CHF the fluid flow first undergoes a transition region characterized by larger vapor pockets, preventing significant heat exchange from the surface to the fluid, eventually leading to film boiling. Once film boiling is encountered, a vapor blanket completely insulates the liquid from the heated surface, causing the wall temperature to continue to rise until eventually the fluid entirely vaporizes and becomes purely single-phase vapor.

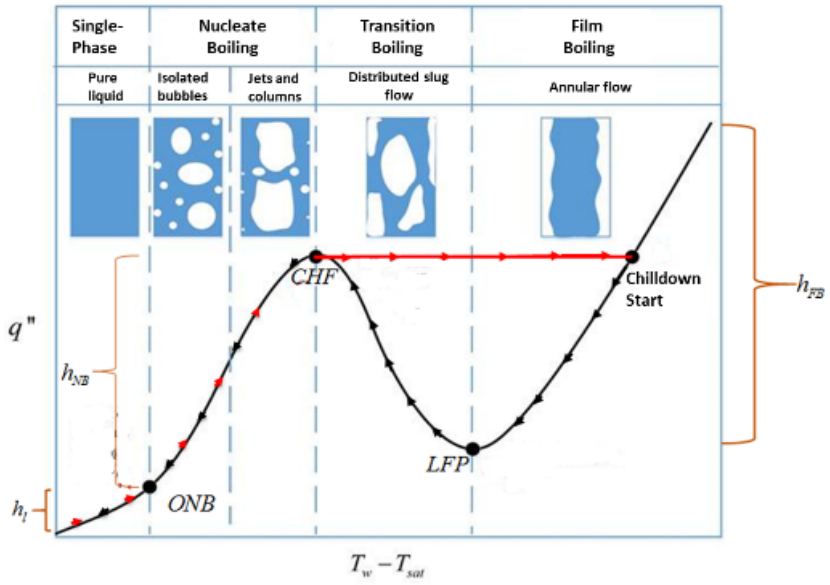

Figure 1: Boiling Curve Taken From [10]

B. Motivation for New Universal Correlations

The development of *new* universal correlations was motivated by a lack of correlations which could be accurately applied to cryogens. Most existing correlations used for two-phase cryogenic flow were developed based on room-temperature fluids and resulted in incredibly high errors when compared to heated configuration flow boiling cryogenic data. Even correlations based on higher saturation temperature cryogens, like nitrogen, have been shown to have poor performance when applied to lower saturation temperature cryogens such as hydrogen. Shown in Figure 2 is a parity plot of LH_2 experimental vs. predicted HTCs for Shah's [11] film boiling correlation which was shown to be one of the best performing correlations during the assessment done by Mercado et al. [3]. Even as the best correlation, the mean absolute error (MAE) was 173% due to most of the film boiling data being underpredicted, as shown.

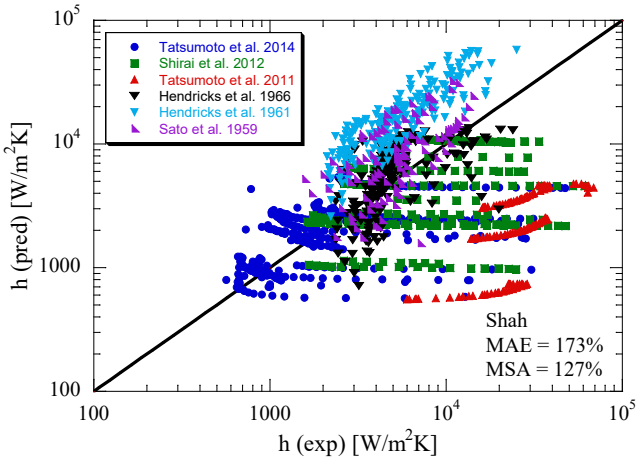

Figure 2: Predicted vs Experimental Film Boiling HTC for Shah's Correlation [11] from [3]

As mentioned previously, popular thermal/fluid solvers such as Thermal Desktop, GFSSP (Generalized Fluid System Simulation Program), and most CFD codes rely on correlations or submodels, despite errors associated with them. For example, it is common practice in cryogenic CFD to rely on a kinetic theory-based mass transfer model that relies on fitting parameters [12]. To improve cryogenic model predictive capabilities specifically in Thermal Desktop

and GFSSP, new universal cryogenic flow boiling correlations have been developed with the goal of covering many different boiling phenomena for several different cryogens. More accurate models will reduce uncertainty, risk, and thus cost when used as design tools for future systems. In this paper, the universal cryogen heated tube flow boiling correlations are ported into TD for an assessment of performance versus the existing in-built correlations. Previous validation exercises have been successfully carried out in GFSSP against liquid nitrogen (LN_2) and liquid methane (LCH_4) [13], LH_2 and liquid helium (LHe) data [14], and Thermal Desktop against LHe [15] and LN_2 and LCH_4 [16] data.

II. Thermal Desktop Model Description

A. Existing Model Infrastructure

The heated tube experiments modeled here are classified as steady state experiments. At the beginning of the experiment, the tube wall and fluid are at the same temperature. Heat is then gradually delivered typically via a heating coil or direct electrification. Once the system reaches steady state at a constant heat flux, the relevant data is collected. Because of the steady state nature, replicating each experimental case is relatively straightforward in Thermal Desktop.

Figure 3 presents a picture of a typical heated tube model in Thermal Desktop. The test sections from the experiments are modeled in Thermal Desktop using a single pipe object. When the pipe element is modeled in Thermal Desktop, a complete thermal-fluid network is created composed of lumps, nodes, conductors, ties, and surfaces based on the pipe properties. The wall nodes of the pipe are defined as diffusion nodes, having a finite thermal mass. When the pipe is created, it is comprised of the same number of nodes, lumps, and ties as the number of temperature sensors as were present in the experiment. The nodes comprising the pipe are evenly spaced, as initial efforts to match the experimental sensor placement resulted in spikes in wall temperate influenced by the pipe length. To determine the temperature at the exact location matching the test sensors, *Measures* were used. Both the inlet and outlet of the pipe are connected to plena lumps via set flow paths, giving control over the fluid flow rate. The *heat load* function was used to simulate the heat flux on the inner surface of the pipe wall.

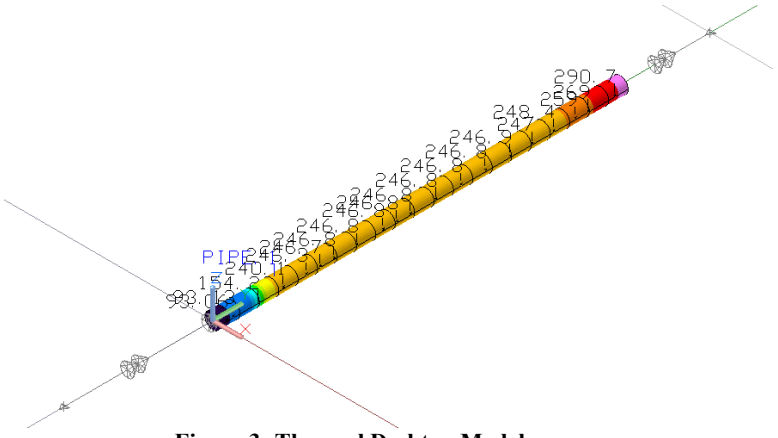

Figure 3: Thermal Desktop Model

In Thermal Desktop, ties dictate the heat transfer between solid nodes and fluid lumps. Ties function similarly to conductors and link the FLUINT/SINDA fluid elements to the Thermal Desktop thermal submodels. The heat transfer through ties is calculated as:

$$QTIE_{tie} = UAM_{tie} \cdot UA_{tie} \cdot \left(T_{node} - TEF_{tie}\right) \tag{1}$$

where $QTIE_{tie}$ is the heat rate through the tie, UA_{tie} is the heat transfer conductance, and T_{node} and TEF_{tie} are the node and effective fluid temperatures. The heat transfer conductance term, UA_{tie}, is a function of the area of heat exchange, A_{tie}, and the heat transfer coefficient, U. UAM_{tie} is a user-defined scaling multiplier set to unity by default. The methods for calculating U are described subsequently.

FLUINT acknowledges two boiling heat transfer regimes by default, nucleate boiling and film boiling [17]. Nucleate boiling is assumed to take place for equilibrium qualities from 0.0 to XNB, which is the cutoff quality for nucleate boiling. XNB is 0.7 by default, which is generally too high for cryogens. An XNB value closer to 0.1 is more

appropriate as Chen's [18] nucleate boiling correlation is unreliable past XNB=0.1 [17]. For qualities between XNB and 1.0, the HTC is found as the interpolation between the nucleate boiling and single-phase vapor correlation predictions.

FLUINT determines the boiling correlation based on a combination of the flow quality and wall superheat. In accordance with Figure 1, the assumption of pure nucleate boiling is invalid beyond the wall temperature at CHF. Above the CHF point, film boiling will persist. At a sufficiently high wall temperature, nucleate boiling ceases to exist altogether. In Thermal Desktop, the point beyond which nucleate boiling ceases correlates to the lowest Leidenfrost temperature, T_{leid}, or the departure from film boiling temperature, T_{dfb}. Table 1 gives the criteria and correlations used in determining the appropriate built-in correlation.

Table 1: FLUINT Boiling Heat Transfer Correlation Matrix

	Low Flow Quality (X<XNB)	**High Flow Quality (XNB<X<1)**
Low Wall Superheat ($T < T_{CHF}$)	Chen [18]	Linear interpolation between Chen [18] and Dittus-Boelter [19]
Transition ($T_{CHF} < T < T_{leid}, T_{dfb}$)	Non-linear interpolation between nucleate and film boiling using scaling laws by Ramilison and Leinhard [22]	Non-linear interpolation between nucleate and film boiling using scaling laws by Ramilison and Leinhard [22]
High Wall Superheat ($T > T_{leid}, T_{dfb}$)	Bromley [23]	Groeneveld [25]

FLUINT uses Chen's nucleate boiling correlation [18] at low equilibrium quality flows, from 0.0 to XNB, with low wall superheats as follows:

$$h_{tp} = Sh_{FZ} + Fh_{DB} \tag{2}$$

The correlation encompasses the interaction of two mechanisms: the macro-convective heat transfer mechanism, which typically operates with moving fluids, and the micro-convective mechanism due to bubble nucleation and growth. The two mechanisms are related using two dimensionless functions: an effective two-phase Reynolds number function F, and a bubble-growth suppression function, S. The correlation was fit to data for water and other organic fluids at qualities between 0.001 and 0.7.

At higher quality flows, XNB<X<1, and low wall superheats ($T < T_{CHF}$), nucleate boiling is no longer dominant. Beyond XNB, HTC is found by the interpolation between Chen's nucleate boiling correlation and single-phase vapor heat transfer approximated by Dittus-Boelter [19]:

$$U = 0.023\,\mathrm{Re}^{0.8}\,\mathrm{Pr}^{0.4}\left(\frac{k}{D}\right) \tag{3}$$

The critical heat flux is found though a modified version of Zuber's pool boiling correlation [20]. The modified correlation is obtained by scaling with the pipe diameter and the estimation as well as a subcooling correction suggested by Gambill [21]:

$$q''_{CHF} = CHFF \cdot \rho_v h_{fg}\left[\frac{\sigma g(\rho_l-\rho_v)}{\rho_v^2}\right]^{\frac{1}{4}}\left(\frac{\rho_l+\rho_v}{\rho_l}\right)^{\frac{1}{2}}(1-\alpha)\left(\frac{D_{8mm}}{D}\right)^{\frac{1}{2}} \tag{4}$$

When the wall temperature is high enough for CHF to be exceeded, transition or film boiling is assumed. The wall temperature must be beyond the Leidenfrost point for full film boiling to be established and maintained. Leidenfrost temperature, T_{leid}, is the point of minimum heat flux on the boiling curve.

$$q''_{MIN-FB} = HFFL \cdot \rho_v h_{fg} \left[\frac{\sigma g \left(\rho_l - \rho_v \right)}{\left(\rho_l + \rho_v \right)^2} \right]^{\frac{1}{4}} \tag{5}$$

At temperatures near the CHF temperature, the approximation above is sometimes too low high and so the lower of T_{leid} and T_{dfb} is used based on estimates from Ramilison and Leinhard [22]:

$$q''_{MIN-FB} = HFFL \cdot \rho_v h_{fg} \left[\frac{\sigma g \left(\rho_l - \rho_v \right)}{\left(\rho_l + \rho_v \right)^2} \right]^{\frac{1}{4}} \tag{6}$$

Beyond the CHF wall temperature but below the Leidenfrost temperature, transition boiling occurs. In the transition boiling regime, the HTC is approximated by a nonlinear interpolation between nucleate and film boiling based on scaling laws proposed by Ramilison and Leinhard [22].

Bromley's correlation [23] for external flow over a horizontal cylinder is used for approximating film boiling at low qualities within ducts or tubes. Bromley's correlation was fit using experimental data for ethyl alcohol, benzene, carbon tetrachloride, and n-hexane. For internal flows the smaller of the subsequent hydraulic diameters is chosen: half the hydraulic diameter, the Helmholtz ("Taylor Instability") wavelength, or the recommendation from Leonard [24].

$$U_{FB} = 0.62 \left[\frac{k_v^3 \rho_v g \left(\rho_l - \rho_v \right) \left(h_{fg} + 0.4 C_{p,v} \Delta T \right)}{L_h \cdot \mu_v \Delta T} \right]^{\frac{1}{4}} \tag{7}$$

Groeneveld's correlation [25] is used at equilibrium quality flows between XNB< X <1, which ensures the HTC is larger than that predicted by the single-phase Dittus-Boelter correlation:

$$U_{FB} = 0.00109 \left\{ \left(\frac{GD}{\mu_g} \right) \left[x + \frac{\rho_g}{\rho_l} (1 - x) \right] \right\}^{0.989} \mathrm{Pr}_g^{1.41} \, Y^{-1.15} \left(\frac{k_g}{D} \right) \tag{8}$$

The logic for calculating the appropriate heat transfer coefficient used by Thermal Desktop is described in Figure 4.

The subroutines dictating flow boiling are not readily accessible by the user in Thermal Desktop. However, the user may adjust variables such as XNB, the CHF scaling parameter (CHFF), and the scaling parameter on Leidenfrost flux/temperature (HFFL) within certain values. A parametric analysis could be conducted on these variables to match existing datasets; however, this would not result in a useful predictive tool for cryogenic applications. Therefore, the default values were left in place for these user accessible parameters in order demonstrate the ability of the purely default correlations as a predictive tool compared to the new universal correlations.

B. Model Infrastructure with New Universal Cryogenic Flow Boiling Correlations

The same fluid network setup from the built-in correlations model was used for the universal correlations Thermal Desktop model. In the universal correlations model, the default HTC between the solid node and fluid lump calculated by SINDA/FLUINT was overridden by that calculated from the universal correlations. The logic of the universal correlations subroutine was originally written in MATLAB, which was ported into Thermal Desktop in a User Code element in a Logic Block.

Figure 5 shows the dynamics between Thermal Desktop and the User Code developed to contain the universal correlations. The initial conditions from each experiment are inputs both to Thermal Desktop and the universal correlations user code. The universal correlation user code then calculates and outputs an HTC for each test point in addition to the location of the critical heat flux (Z_{CHF}). The built-in Thermal Desktop solver then takes the resultant HTC and computes the fluid state variables (temperature, pressure, etc.), wall temperatures, and axial conduction

between the solid nodes. This process repeats as the model iterates until the convergence criteria is met. The convergence criteria was 0.001 K for every run.

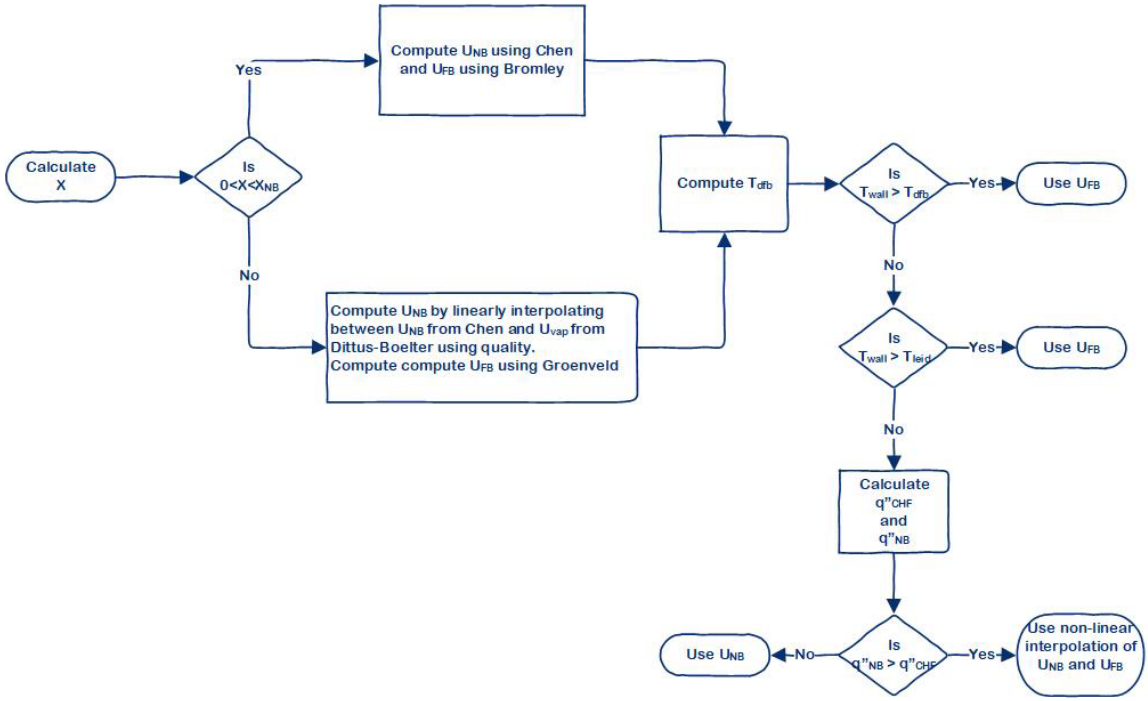

Figure 4: Logic Tree for Selecting Built-in Heat Transfer Coefficient in Thermal Desktop

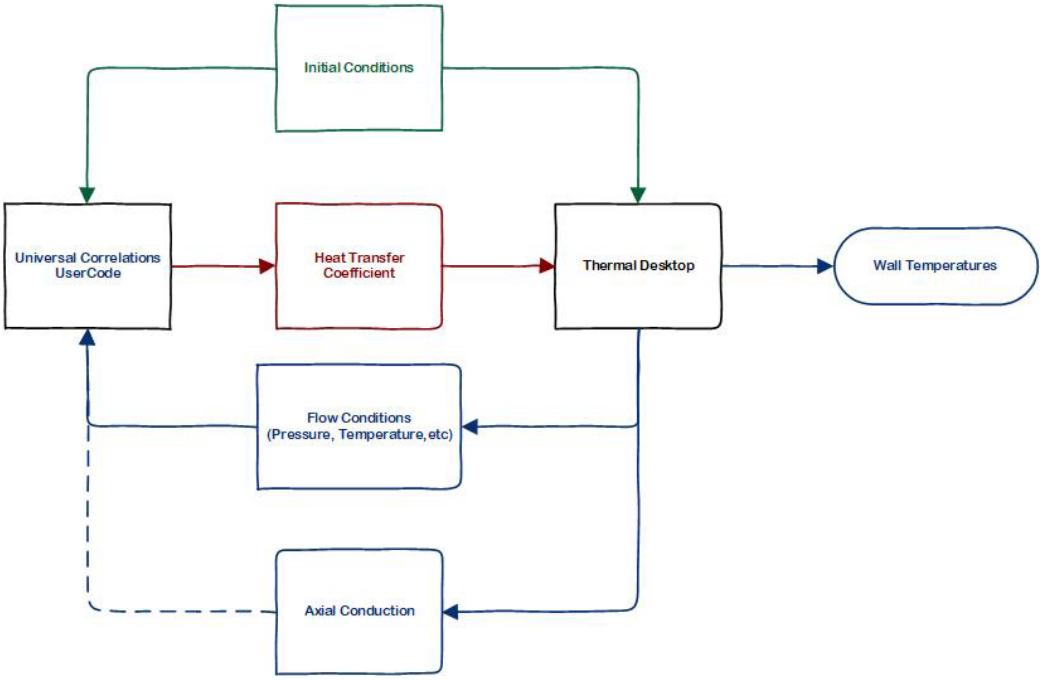

Figure 5: Flow Diagram of Universal Correlations Implantation into Thermal Desktop

The universal correlations and original code have provisions for pressure drop and axial conduction through the test section pipe [22]. The pressure drop routines used by Thermal Desktop cannot be easily altered or overwritten.

Since this code is made to work in collaboration with Thermal Desktop and SINDA/FLUINT, neither the pressure drop nor axial conduction portions of the correlations were implemented, because Thermal Desktop contains its own solvers for these components.

The universal correlations have amendments to handle two CHF mechanisms: departure from nucleate boiling-type (DNB) and dryout-type. The fluid flow characteristics of each are shown in Figure 6. DNB generally occurs with high mass flux and high heat flux and leads to bubbly flow in the pre-CHF region. Meanwhile, dryout-type CHF occurs with low mass flux and low heat fluxes, and first leads to bubbly flow which is followed by annular flow in the pre-CHF region.

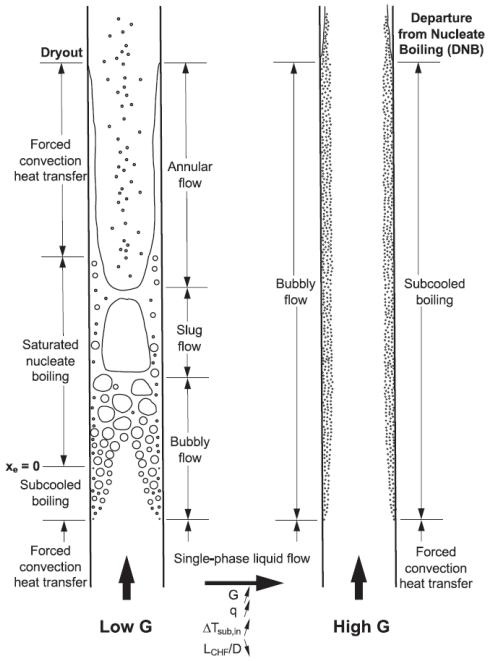

Figure 6: Flow Patterns Leading to CHF due to Dryout-Type and DNB-Type in a Uniformly Heated Tube, from [5]

To find the z_{CHF} location, a heat flux for the conditions q''_{DNB} and q''_{Dryout}, respectively, was calculated based on the given local fluid properties. The calculated heat flux conditions are then compared to a constant boundary condition heat flux (q''_{wall}). The point where q''_{wall} surpasses q''_{DNB} or q''_{Dryout} is found to be z_{CHF}. In cases where both q''_{DNB} and q''_{Dryout} fall under q''_{wall}, the z_{CHF} found from q''_{Dryout} was chosen. A modification was made to q''_{wall} to deal with cases where the code was incorrectly predicting z_{CHF} past the length of the pipe (neither q''_{DNB} nor q''_{Dryout} intersect q''_{wall}). Equations 9 and 10 scale the wall heat flux, resulting in $q''_{lower\ bound}$ and $q''_{upper\ bound}$:

$$q''_{upper\ bound} = q''_{wall}\left(1+0.25\left(\frac{Z}{L}\right)^2\right) \tag{9}$$

$$q''_{lower\ bound} = q''_{wall}\left(1-0.25\left(\frac{Z}{L}\right)^2\right) \tag{10}$$

Only $q''_{upper\ bound}$ was used in finding Z_{CHF}, meaning the intersection between q''_{DNB} or q''_{Dryout} and $q''_{upper\ bound}$ was determined to be the z_{CHF} location. This process is illustrated in Figure 7 for Lewis et al. [9] Nitrogen Run 280. Here, the code finds locations that meet the criteria for both DNB and Dryout, so the code selected the location corresponding to DNB at 0.256 m.

To account for the connection of the CHF point with the film boiling regime, a hyperbolic tangent function was used to blend the last pre-CHF HTC with the local post-CHF coefficient as shown in Equation 11. The blending

heat transfer coefficient, $h_{tp,\ patched}$, was calculated and used for the entire post-CHF length of the pipe. A blending coefficient, φ, of 5 was used for runs in this paper.

$$\frac{1}{h_{tp,patched}} = \frac{1}{h_{tp,pre-CHF}} + \frac{1+\tanh\left(\varphi\left(z-z_{CHF}\right)\right)}{2}\left(\frac{1}{h_{tp,\text{post-CHF}}} - \frac{1}{h_{tp,pre-CHF}}\right) \tag{11}$$

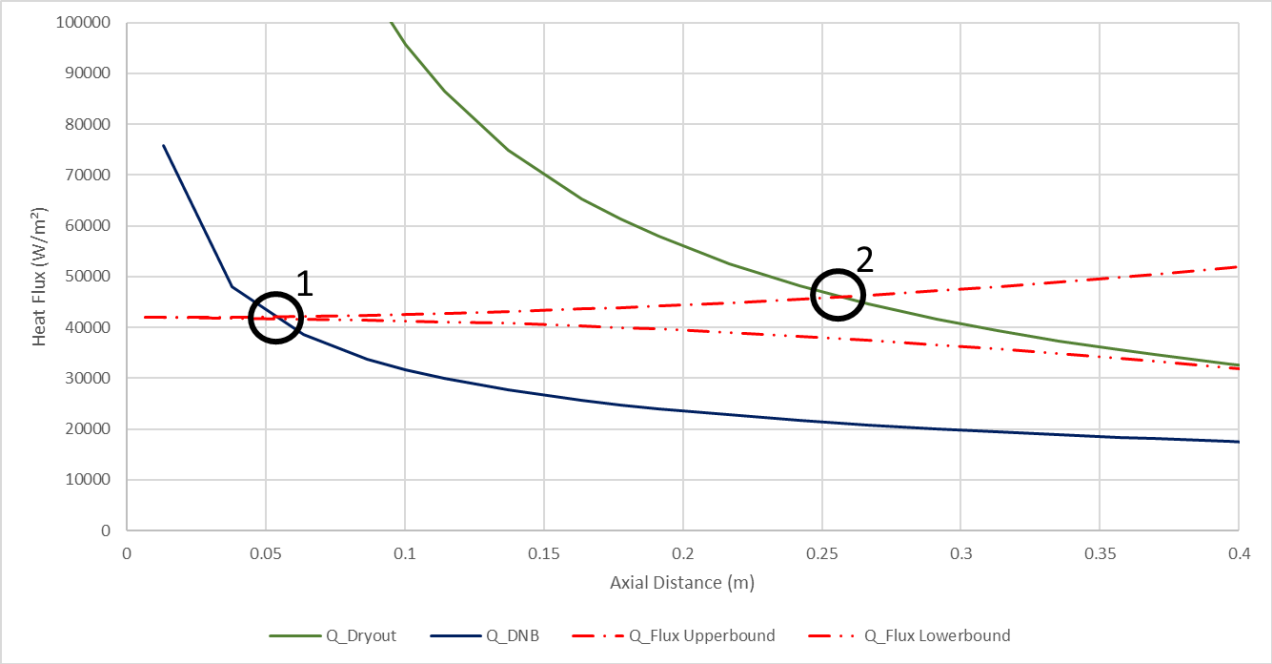

Figure 7: Heat Flux as a Function for z_{CHF} Calculation for Lewis et al. [9] Nitrogen Run 280

III. Test Matrix and Model Versions

Tables 2 and 3 show the test matrix of simulations for Lewis et al. [9] and Hendricks et al. [8], respectively. Before presenting results, it is important to briefly discuss the different versions of the models that were run. Both the wall temperature along the pipe and the location of z_{CHF} were of interest to compare between the model and data. However, an error in the predicted location of z_{CHF} compounds error in the predicted post-CHF downstream wall temperature. For example, if z_{CHF} in the model is predicted significantly downstream of the actual z_{CHF}, then there are a significant number of datapoints where the model and the experiment are in different flow regimes. The large wall temperature difference between nucleate and film boiling regimes (film boiling wall temperatures often being 10 times as large as nucleate boiling wall temperatures) is therefore compounded by any error in the predicted location of z_{CHF}. Therefore, two versions of the Thermal Desktop model with universal cryogenic flow boiling correlations were used: the '*Calculated* z_{CHF}' model where the code must determine the location of z_{CHF} and the '*Fixed* z_{CHF}' model where the experimental location of CHF was input into the code. The latter allows for a direct comparison of nucleate boiling data to nucleate boiling models, and film boiling data to film boiling models. Therefore, in total, three versions of the model were run: (1) Calculated z_{CHF} with new universal correlations, (2) Fixed z_{CHF} with new universal correlations, and (3) Calculated z_{CHF} model with built-in correlations.

Author	Year	Case	Fluid	Pipe Material	$x_{e,in}$	T_{in} (K)	P_{in} (MPa)	q" (W/m^2)	G (kg/m^{2}s)	# of points	z_{CHF} (mm)
Lewis et al. [9]	1962	Run 127	LH_2	SS304	-0.02460	22	0.2068	38644	4.028	13	42.3
Lewis et al. [9]	1962	Run 137	LH_2	SS304	-0.02038	24.61	0.3447	32492	5.479	13	169.2
Lewis et al. [9]	1962	Run 140	LH_2	SS304	-0.02219	24.56	0.3447	29338	5.561	13	222.7
Lewis et al. [9]	1962	Run 146	LH_2	SS304	-0.04144	24.06	0.3516	58991	14.78	13	-
Lewis et al. [9]	1962	Run 147	LH_2	SS304	-0.05061	25.94	0.5033	70663	17.36	13	-

Lewis et al. [9]	1962	Run 148	LH_2	SS304	-0.05495	25.83	0.5033	67508	13.14	13	-
Lewis et al. [9]	1962	Run 149	LH_2	SS304	-0.02135	26.5	0.4895	79180	14.38	7	-
Lewis et al. [9]	1962	Run 150	LH_2	SS304	-0.00482	26.89	0.4895	76657	14.58	13	-
Lewis et al. [9]	1962	Run 158	LH_2	SS304	-0.05670	23.56	0.3516	66562	10.97	13	-
Lewis et al. [9]	1962	Run 159	LH_2	SS304	-0.05172	23.83	0.3585	69716	17.77	13	-
Lewis et al. [9]	1962	Run 160	LH_2	SS304	-0.04993	24.11	0.3723	49843	7.093	13	-
Lewis et al. [9]	1962	Run 161	LH_2	SS304	-0.10515	21.83	0.3516	55521	8.707	13	-
Lewis et al. [9]	1962	Run 162	LH_2	SS304	-0.03294	21.67	0.2068	60884	18.31	13	-
Lewis et al. [9]	1962	Run 163	LH_2	SS304	-0.03536	21.72	0.2137	77603	18.31	13	-
Lewis et al. [9]	1962	Run 164	LH_2	SS304	-0.05511	23.72	0.3585	57098	8.219	13	-
Lewis et al. [9]	1962	Run 165	LH_2	SS304	-0.05342	23.78	0.3585	66246	11.77	13	-
Lewis et al. [9]	1962	Run 166	LH_2	SS304	-0.10448	21.72	0.3447	66246	11.38	13	-
Lewis et al. [9]	1962	Run 167	LH_2	SS304	-0.11314	21.67	0.3585	57098	7.825	13	-
Lewis et al. [9]	1962	Run 168	LH_2	SS304	-0.18392	21.67	0.4895	43218	10.01	13	-
Lewis et al. [9]	1962	Run 169	LH_2	SS304	-0.18392	21.67	0.4895	41956	11.05	13	-
Lewis et al. [9]	1962	Run 170	LH_2	SS304	-0.08927	24.5	0.4757	43218	20.61	13	-
Lewis et al. [9]	1962	Run 171	LH_2	SS304	-0.05014	25.22	0.4482	58991	9.521	13	-
Lewis et al. [9]	1962	Run 172	LH_2	SS304	-0.05513	25.26	0.4826	68455	11.45	13	-
Lewis et al. [9]	1962	Run 306	LH_2	SS304	-0.03464	23.94	0.3309	51735	10.84	15	101.5
Lewis et al. [9]	1962	Run 311	LH_2	SS304	-0.06043	23.5	0.3558	56309	18.15	15	105.7
Lewis et al. [9]	1962	Run 313	LH_2	SS304	-0.07581	22.89	0.3509	49369	21.97	15	70.5
Lewis et al. [9]	1962	Run 317	LH_2	SS304	-0.04170	24.17	0.3592	40852	5.181	15	122.6
Lewis et al. [9]	1962	Run 322	LH_2	SS304	-0.00106	25.33	0.3551	57256	11.80	15	35.2

Table 2: Test Matrix for Simulations of Lewis et al. (1962) [9] Cases

Author	Year	Case	Fluid	Pipe Material	$x_{e,in}$	T_{in} (K)	P_{in} (MPa)	q'' (W/m^2)	G (kg/m^2s)	# of points	z_{CHF} (mm)
Hendricks et al. [8]	1966	Run 1-1146	LH_2	Inconel X	-0.0851	28.33	0.7598	1.19e6	327.4	12	-
Hendricks et al. [8]	1966	Run 3-1143	LH_2	Inconel X	-0.0717	28.39	0.7433	7.35e5	329.4	12	-
Hendricks et al. [8]	1966	Run 4-1251	LH_2	Inconel	-0.3107	25.5	0.8687	8.17e5	531.9	12	-
Hendricks et al. [8]	1966	Run 1-542	LH_2	SS304	-0.2295	22.67	0.6164	1.36e6	1237	12	-
Hendricks et al. [8]	1966	Run 2-541	LH_2	SS304	-0.4249	22.56	0.8612	1.32e6	1119	12	-
Hendricks et al. [8]	1966	Run 6-201	LH_2	SS304	-0.5588	27.33	1.113	1.73e6	1146	12	-
Hendricks et al. [8]	1966	Run 7-540	LH_2	SS304	-0.3241	22.83	0.7598	2.09e6	1179	12	-
Hendricks et al. [8]	1966	Run 9-204	LH_2	SS304	-0.1784	27.28	0.8129	1.63e6	1122	12	-
Hendricks et al. [8]	1966	Run 10-535	LH_2	SS304	-0.2370	23.78	0.6853	1.80e6	945.2	12	-
Hendricks et al. [8]	1966	Run 11-536	LH_2	SS304	-0.2761	23.89	0.7467	2.08e6	932.5	12	-
Hendricks et al. [8]	1966	Run 2-1247	LH_2	Inconel	-0.6451	25.72	1.103	1.31e6	536.6	12	-

Table 3: Test Matrix for Simulations of Hendricks et al. (1966) [8] Cases

It should also be noted that 8 of the 28 Lewis et al. [9] cases listed no z_{CHF}, indicating that the transition to film boiling occurred before the first temperature sensor in the experiment. To preserve the blending function in the model, an additional test point was inserted into the model halfway between the inlet and the first sensor. For the Fixed z_{CHF} models, z_{CHF} was placed immediately after this first test point, allowing the HTC of this first point to serve as the pre_{CHF} HTC in the blending region. For Hendricks et al. [8], z_{CHF} was set to 0.0 mm in the Fixed z_{CHF} model, and no blending was used.

To determine the performance of the models, mean absolute percentage error (MAPE), symmetric mean absolute percentage error (SMAPE), and z_{CHF} % error are used and defined as follows:

$$MAPE = \frac{|E - M|}{E} x100 \tag{12}$$

$$SMAPE = \frac{|E - M|}{(E + M)/2} x100 \tag{13}$$

$$Z_{CHF}\,\%\,Error = \frac{|Z_{CHF,data} - Z_{CHF,\mathrm{model}}|}{L} x100 \tag{14}$$

The MAPE is a classical metric used throughout two-phase flow literature. The SMAPE is used to equally penalize over- and underpredictions, since the SMAPE bounds lie between 0% and 200%. If there are not extreme overpredictions or underpredictions, MAPE and SMAPE tend to produce very similar results. The error in the location of CHF is also tracked using Equation 14. Note that for Fixed z_{CHF}, only the model with universal correlations is compared against the data. For each test case, where applicable (i.e. not every single test case had all possible flow

boiling regimes), for both 'Calculated z_{CHF}' and 'Fixed z_{CHF}' cases, MAPE and SMAPE were tabulated for pre-ONB, nucleate boiling, and film boiling points. For subsequent parity plots, +/- 30% (θ) and +- 50% (φ) error bands on the data are plotted alongside the data and model prediction.

IV. Results and Discussion

A. Lewis et al. 1962 [9] Hydrogen Results

Lewis et al. [9] conducted a comprehensive study on LH_2 and LN_2 flow boiling in the vertical upflow configuration on a 1.4 cm diameter, 0.41 m long tube. Of the available tests, 28 LH_2 cases were chosen for model validation. Figure 8 plots the experimental and predicted wall temperature as a function of axial distance using the Calculated z_{CHF} model using either the built-in or universal cryogenic flow boiling correlations for Run 137. Figure 9 plots results for Run 137 using the Fixed z_{CHF} model. Run 137 is for relatively low mass flux and low heat flux. As shown in Figure 8 where the model must determine the location of CHF, neither version of the model precisely predicts the location. However, the model with universal correlations does a significantly better job, with an error in z_{CHF} of 10% whereas for built-in correlations, the error is over 4 times higher (~45%). The model with built-in correlations drastically overpredicts the wall temperature in the nucleate boiling regime, and conversely drastically underpredicts the wall temperature in the film boiling regime. Meanwhile, the model with universal correlations precisely predicts wall temperature in nucleate boiling and predicts well the temperature in film boiling. Most of the error in the model using the universal correlations is attributed to the discrepancy in the location of z_{CHF} (two points the model predicts are in nucleate boiling whereas the data indicates film boiling).

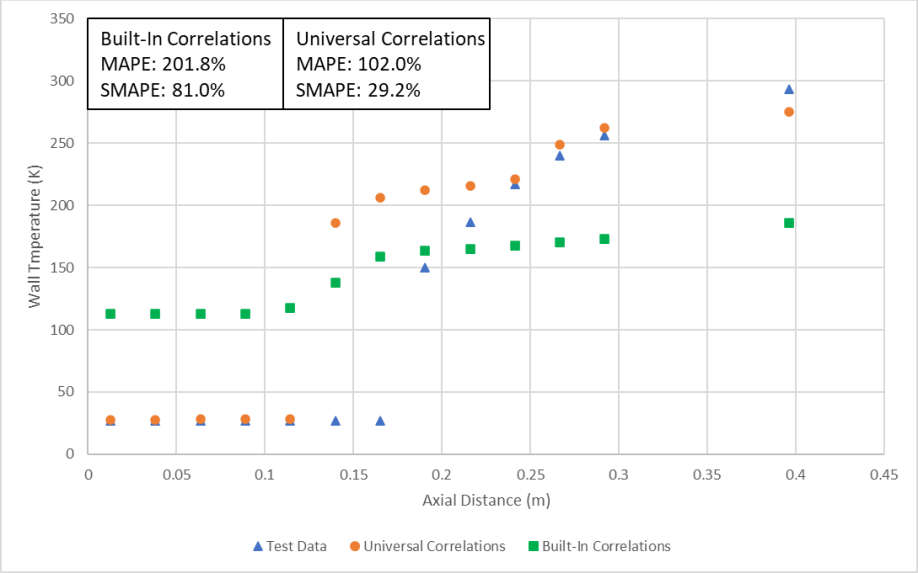

Figure 8: Experimental Versus Predicted Wall Temperature as a Function of Distance along the Pipe for Lewis et al. 1962 [9] Hydrogen, Run 137, using Calculated z_{CHF} Models

For Run 137 in Figure 9, when fixing the location of CHF, the model predicts the magnitude of the wall temperature for nucleate boiling precisely for all points. For film boiling, the first data point is slightly overpredicted and the final data point is slightly underpredicted, but the others are well predicted. Overall, for Fixed z_{CHF}, the model predicts the data within 3% and 8% for nucleate and film boiling, respectively.

Figure 10 plots the experimental and predicted wall temperature as a function of axial distance using the Calculated z_{CHF} model using either the built-in or universal cryogenic flow boiling correlations for Run 317. Figure 11 plots results for Run 317 using the Fixed z_{CHF} model. Run 317 is for relatively low mass flux and moderate heat flux. As with Run 137, the Calculated z_{CHF} model with built-in correlations tends to overpredict nucleate boiling wall temperature and underpredict film boiling wall temperature. Meanwhile, the Predicted z_{CHF} model with universal correlations predicts nucleate boiling well but tends to over-predict the film boiling wall temperature; disparity between the data and model diminishes as a function of distance along the tube post-CHF. The overall error is nearly half using the model with universal correlations over the built-in correlations (36% versus 69% SMAPE). Meanwhile,

Figure 11 shows that fixing the location of CHF reduces the error post-CHF. The MAPE is 28% and 15% for nucleate boiling and film boiling points, respectively.

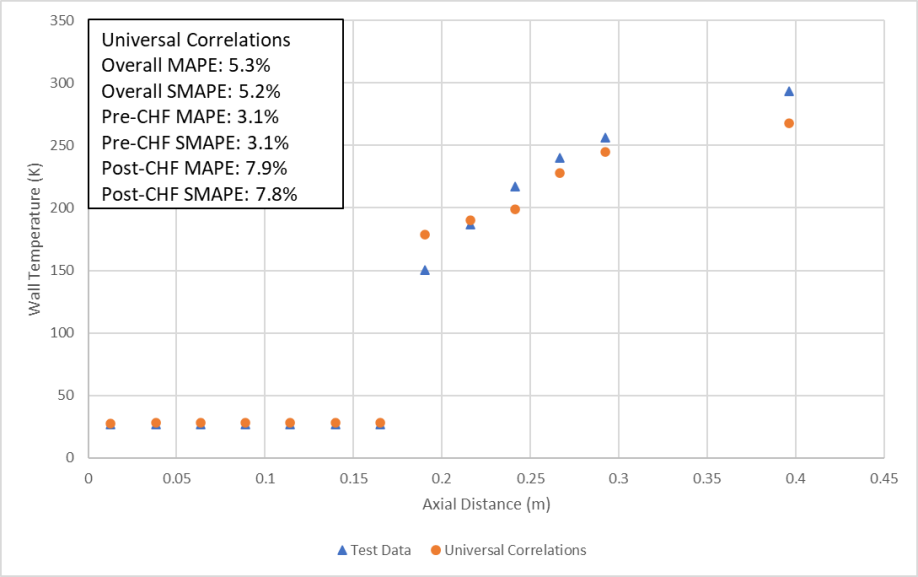

Figure 9: Experimental Versus Predicted Wall Temperature as a Function of Distance along the Pipe for Lewis et al. 1962 [9] Hydrogen, Run 137, using Fixed z_{CHF} Model

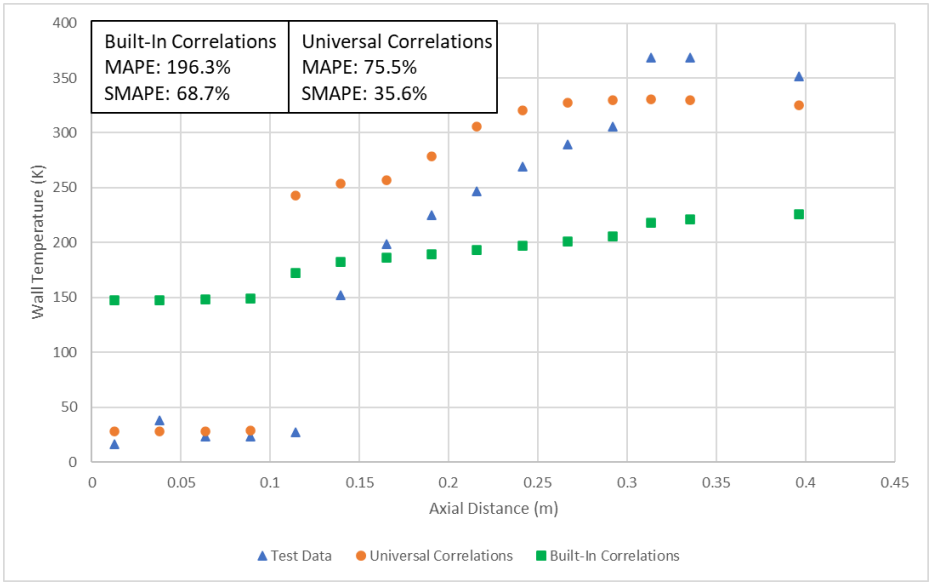

Figure 10: Experimental Versus Predicted Wall Temperature as a Function of Distance along the Pipe for Lewis et al. 1962 [9] Hydrogen, Run 317, using Calculated z_{CHF} Models

Figure 12 presents a parity plot for all Calculated z_{CHF} model runs for Lewis et al. [9] using either the built-in or universal correlations. First, the model with universal correlations has slightly higher SMAPE than MAPE; this is due to the slight tendency of the model to underpredict the wall temperature. Examination of the case-by-case results indicates this underprediction is mostly attributed to z_{CHF} being predicted downstream of the test data, meaning a nucleate boiling correlation would be compared against some film boiling datapoints. Meanwhile, the model with built-in correlations has higher MAPE by 23% but lower SMAPE by 12%.

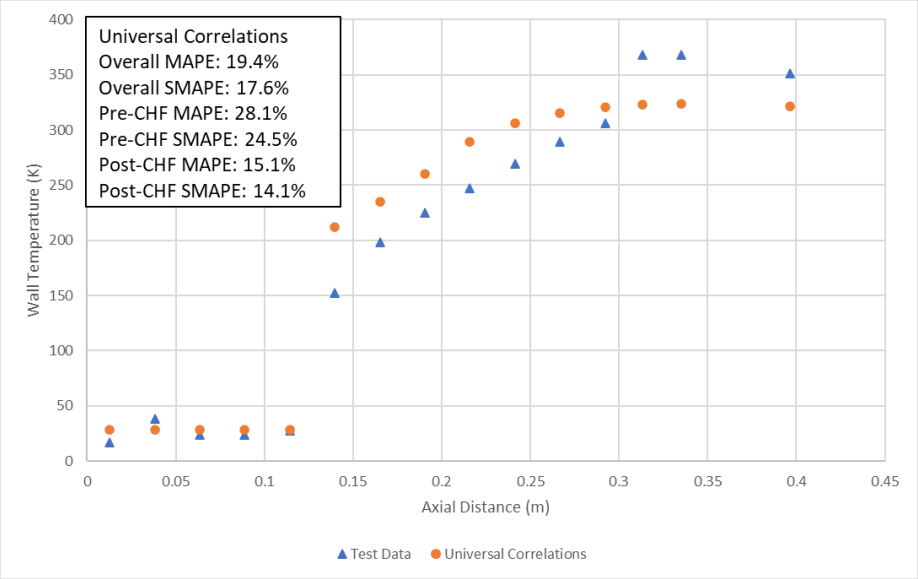

Figure 11: Experimental Versus Predicted Wall Temperature as a Function of Distance along the Pipe for Lewis et al. 1962 [9] Hydrogen, Run 317, using Fixed z_{CHF} Model

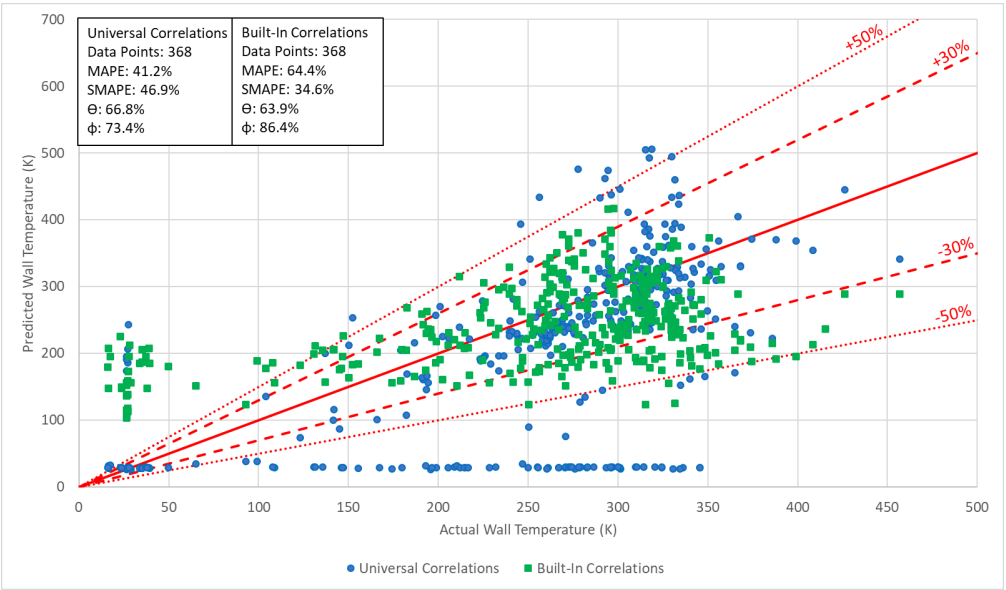

Figure 12: Lewis et al. 1962 [9] Hydrogen Universal Correlations vs Built-In Correlations, Calculated z_{CHF} Parity Plot

Figures 13 and 14 present parity plots for all Fixed z_{CHF} model runs for [9] using the universal correlations. As shown, the error values are below 17% for nucleate boiling points and below 19% for film boiling points. Comparing Calculated versus Fixed z_{CHF} runs for the model with universal correlations, it is clear that the largest discrepancies and cause of error is the disparity between data and model just post-CHF. The blending function parameters were chosen to provide a conservative post-CHF prediction [27], thus the predicted wall temperature tends to be higher than the data.

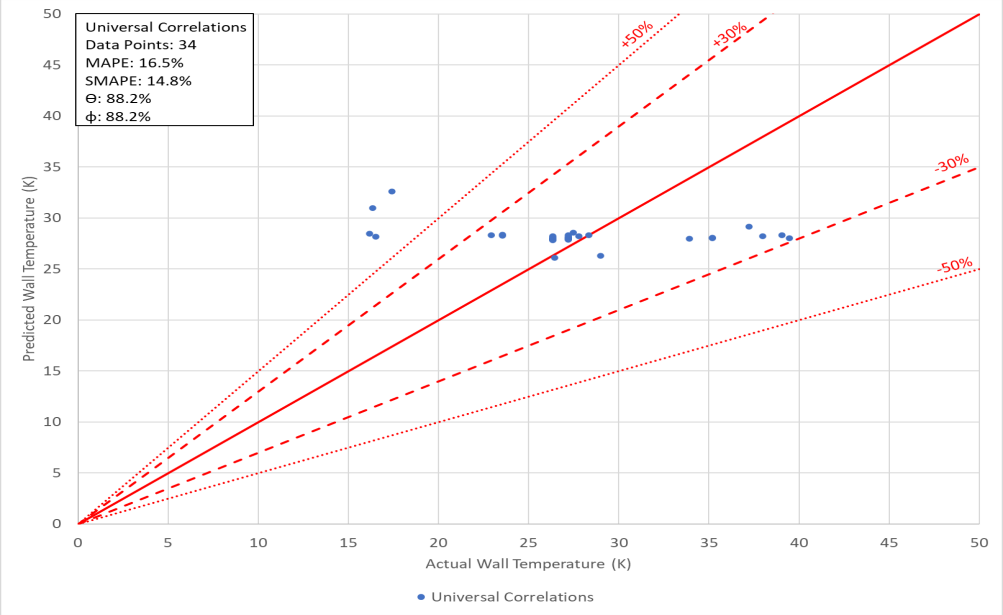

Figure 13: Lewis et al. (1962) [9] Hydrogen Universal Correlations, Fixed z_{CHF} Model, Nucleate Boiling Parity Plot

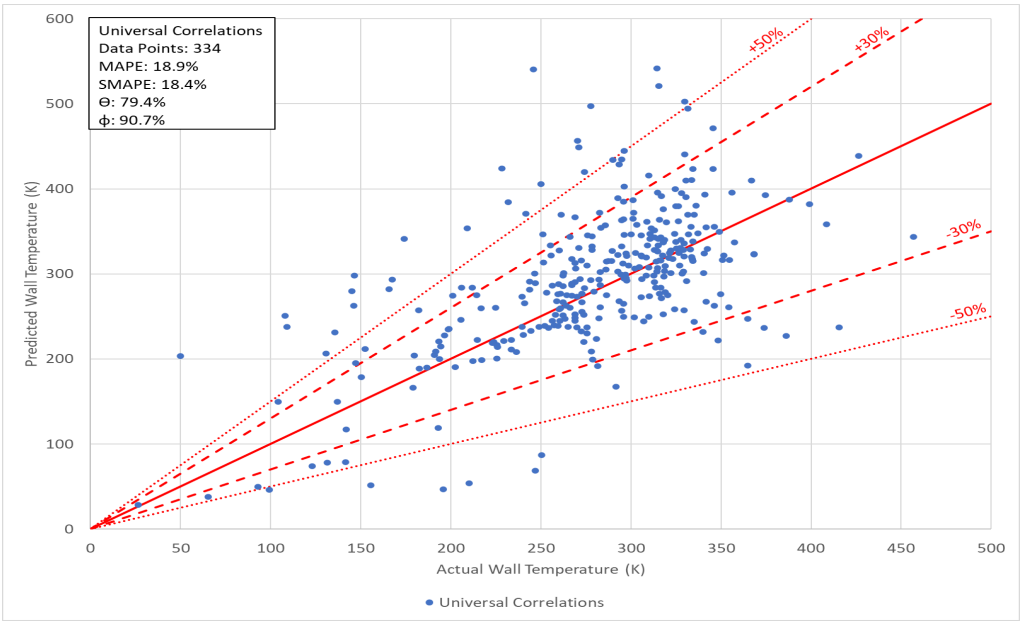

Figure 14: Lewis et al. (1962) [9] Hydrogen Universal Correlations, Fixed z_{CHF} Model, Film Boiling Parity Plot

B. Hendricks et al. [8] Hydrogen Results

Hendricks et al. [8] published multiple papers on LH_2 boiling in the 1960s and 1970s on various Inconel and SS304 tubes. Most of the testing was in the vertical upflow configuration. In Hendricks et al. [8], local HTC and pressure drop data were taken from 11 cases in a vertical upflow orientation on a 0.61 m long tube. The data predominately focused on the film boiling regime. Note that the majority of the data was actually subcooled film boiling data. Also note that in these datasets, z_{CHF} occurred before the first datapoint for all runs, which was accurately predicted by both the built-in and universal correlations for all runs. Lastly, note that since all of the points examined here are in film boiling, there is no difference between Calculated z_{CHF} and Fixed z_{CHF} model results.

Figure 15 plots results for Run 1-1146 for the Calculated z_{CHF} models using both built-in and universal correlations against the data. Run 1-1146 is for relatively low mass flux and intermediate heat flux. As shown, both the model with built-in correlations and model with universal correlations underpredicts the film boiling data. The model with built-in correlations levels out nearly halfway along the tube despite changes in the experimental temperature. Meanwhile, better agreement is obtained for the model with universal correlations, particularly as a function of distance along the tube. The spike in the model is at the location where x_e transitions to saturation. For this case, the MAPE and SMAPE are 2 and 2.4 times larger for built-in over universal correlations, respectively. The largest discrepancy appears to be for the central nodes.

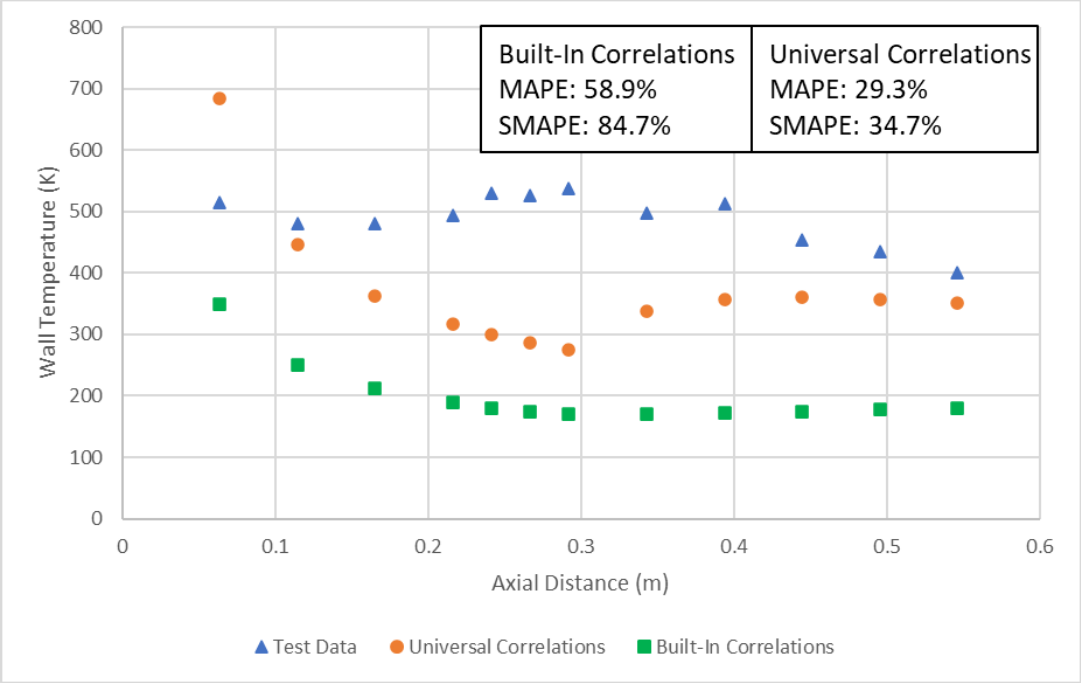

Figure 15: Experimental Versus Predicted Wall Temperature as a Function of Distance along the Pipe for Hendricks et al. 1966 [8] Hydrogen, Run 1-1146, using Calculated z_{CHF} Models

Figure 16 plots results for Run 9-204 for the Calculated z_{CHF} models using both built-in and universal correlations against the data. Run 9-204 is for relatively high mass flux and intermediate heat flux. As shown, both models tend to underpredict the data, except at the beginning and end of the tube. For this case, the model with built-in correlations slightly outperforms the model with universal correlations. Both versions perform better here than for the low flow case of Run 1-1146.

Figure 17 shows a parity plot for Calculated z_{CHF} model runs using either built-in or universal correlations for all data from Hendricks et al. [8]. As shown, the model with built-in correlations slightly outperforms the model with universal correlations by 3% MAPE. The plot shows that a large percentage of data for both models is underpredicted. The main drawback for the model with universal correlations is that there is no subcooled film boiling model available. The inlet state for all runs from Lewis et al. [9] was subcooled; as such the model evaluates film boiling correlations using subcooled properties. Despite this fact, the model with universal correlations tends to have better agreement with the data post-CHF, particularly farther downstream. What appears to skew the results is the disparity between data and model for datapoints near the inlet of the tube. In both Hendricks et al. [8] and Lewis et al. [9], there are many subcooled film boiling datapoints.

To examine this impact of subcooled film boiling error, the results were again compiled, but excluding the subcooled film boiling datapoints. Results are shown in Figures 18, 19, and 20 for Hendricks et al. [8] and Lewis et al. [9] Calculated z_{CHF} and Fixed z_{CHF}, respectively. As shown in Figure 18, removing the subcooled film boiling points lowers the MAPE and SMAPE for universal correlations by 6% and 13%, respectively for Hendricks et al. [8]. Meanwhile, the error values increase slightly for the model with built-in correlations. Thus, the model with universal correlations outperforms the model with built-in correlations when removing points that the model was not intended to be used. Meanwhile, for Lewis et al. [9], comparing Figures 12 and 19, the MAPE and SMAPE values decrease by a few points for the Calculated z_{CHF} model with universal correlations. Likewise, comparing Figures 14 and 20, the

MAPE and SMAPE decrease slightly for Lewis et al. [9] cases for the Fixed z_{CHF} model with universal correlations. For Calculated z_{CHF} models, the main cause of remaining error is due to error in predicting the exact location of z_{CHF}.

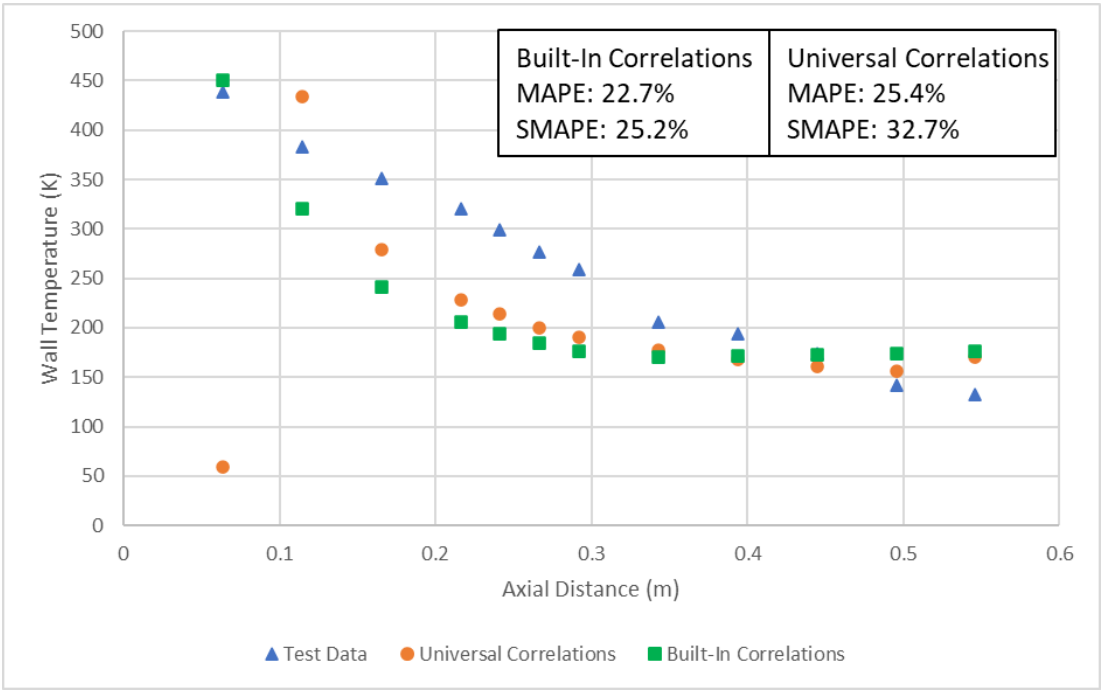

Figure 16: Experimental Versus Predicted Wall Temperature as a Function of Distance along the Pipe for Hendricks et al. 1966 [8] Hydrogen, Run 9-204, using Calculated z_{CHF} Models

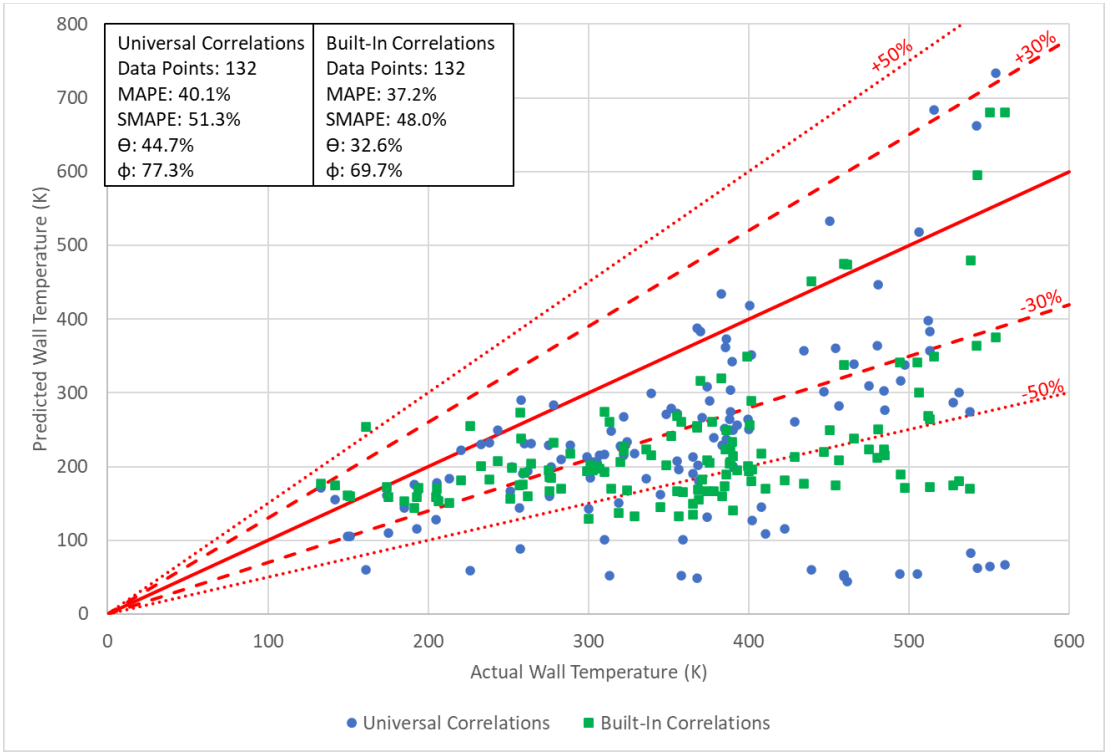

Figure 17: Hendricks et al. [8] Hydrogen Universal Correlations vs Built-In Correlations Calculated z_{CHF} Parity Plot Including Subcooled Film Boiling Points

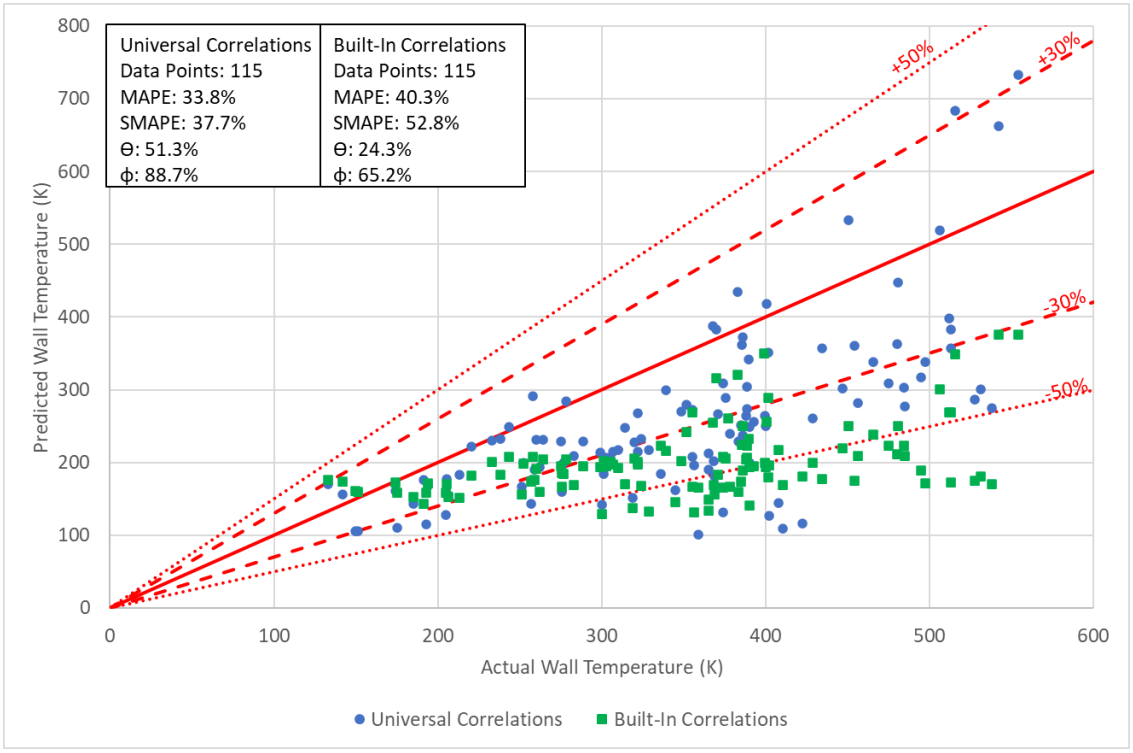

Figure 18: Hendricks et al. [8] Hydrogen Universal Correlations vs Built-In Correlations, Calculated z_{CHF} Parity Plot Excluding Subcooled Film Boiling Points

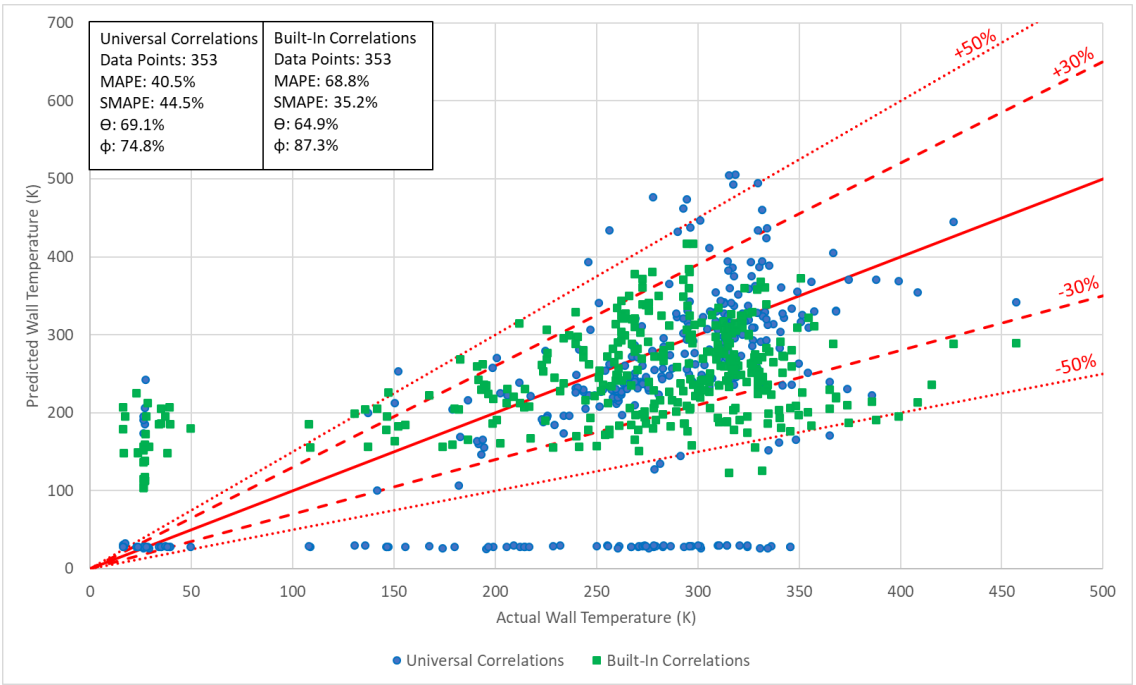

Figure 19: Lewis et al. [9] Hydrogen Universal Correlations vs Built-In Correlations, Calculated z_{CHF} Parity Plot Excluding Subcooled Film Boiling Points

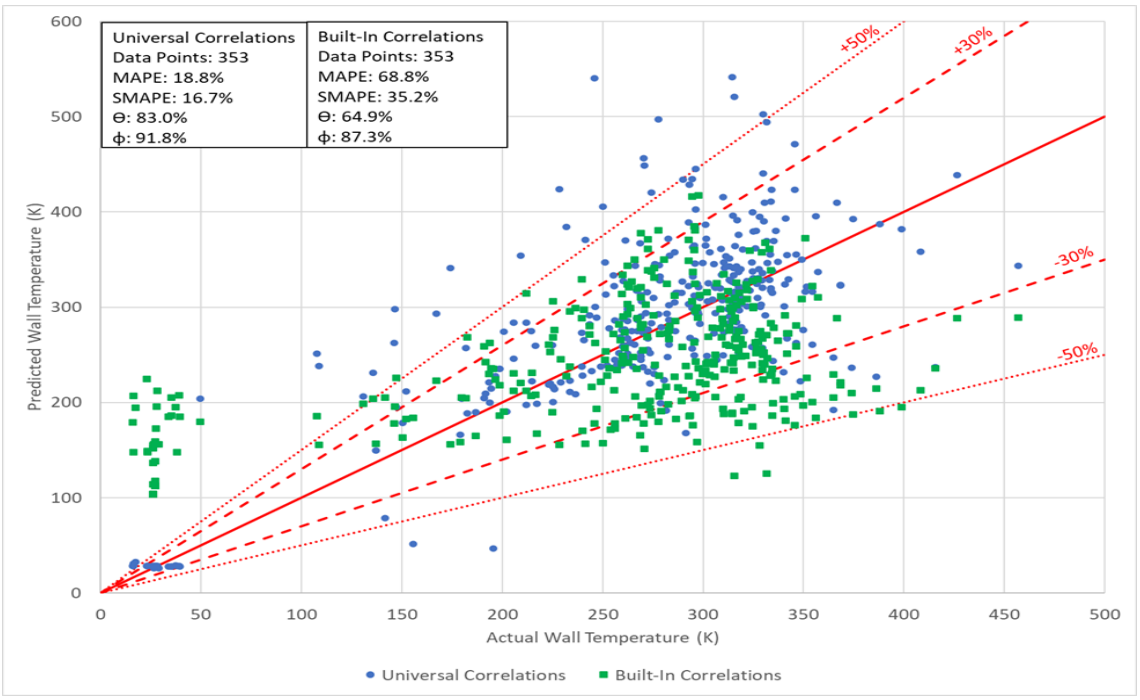

Figure 20: Lewis et al. [9] Hydrogen Universal Correlations vs Built-In Correlations, Fixed z_{CHF} Parity Plot Excluding Subcooled Film Boiling Points.

V. Conclusion

Developing accurate models of various cryogenic propellant transfer phenomena will reduce risk and reduce margins in the design of future in-space cryogenic propellant vehicles. The majority of current tools used to model cryogenic transfer phenomena are predominately anchored to room temperature fluids and have demonstrated numerous times to exhibit poor predictive performance. This paper presented a comparison of the performance of two separate subroutines utilized by Thermal Desktop for modeling steady state cryogenic flow boiling in heated tubes. The built-in correlations were compared against the recently developed universal cryogenic flow boiling heat transfer correlations that have been anchored to the largest available set of cryogenic flow boiling datapoints in the world. To compliment recent validation exercises performed on liquid helium [15] and liquid nitrogen and liquid methane cases [16], both sets of correlations were compared against two separate liquid hydrogen data sets from [8, 9]. The two data sets spanned a wide range of inlet conditions, mass flux, and heat flux. For the model with universal correlations, two versions of the code were run, one where Thermal Desktop determined the location of the critical heat flux (Calculated z_{CHF}) and one where the location of critical flux was fed into the model (Fixed z_{CHF}).

Tables 4 and 5 compile all results when including and excluding subcooled film boiling points, respectively. As shown, when including subcooled film boiling, the model with universal correlations outperforms the model with built-in correlations for Lewis et al. [9], but the model with built-in correlations slightly outperforms the model with universal correlations for Hendricks et al. [8]. However, when excluding subcooled film boiling points, the model with universal correlations outperforms the model with built-in correlations for both cases. For Fixed z_{CHF} model runs, the model with universal correlations yields error values < 20% for Lewis et al. [9] and < 38% for Hendricks et al. [8]. Overall, the Thermal Desktop model with the new universal cryogenic flow boiling correlations demonstrates an improvement in predictive performance over the Thermal Desktop model using built-in correlations for both wall temperature and location of critical heat flux compared to the data for LH_2 flow boiling in heated tubes. Thus, Thermal Desktop with the new universal cryogenic flow boiling correlations can be used to model, design, and optimize a wide variety of current and future cryogenic propellant transfer system applications.

	Built-in Correlations		Universal Correlations Including Subcooled Film Boiling					
	Overall		Calculated Z_{CHF}		Fixed Z_{CHF}			
Author	MAPE	SMAPE	MAPE	SMAPE	NB MAPE	NB SMAPE	FB MAPE	FB SMAPE
Lewis et al. [9]	64.4%	34.6%	41.2%	46.9%	16.5%	14.8%	18.9%	18.4%
Hendricks et al. [8]	37.2%	48.0%	40.1%	51.3%	-	-	40.1%	51.3%

Table 4: Compiled Results for Calculated and Fixed z_{CHF} Models when Including Subcooled Film Boiling Points

	Built-in Correlations		Universal Correlations Excluding Subcooled Film Boiling			
	Overall		Calculated z_{CHF}		Fixed z_{CHF}	
Case	MAPE	SMAPE	MAPE	SMAPE	MAPE	SMAPE
Lewis et al. [9]	68.8%	35.2%	40.5%	44.5%	18.8%	16.7%
Hendricks et al. [8]	40.3%	52.8%	33.8%	37.7%	33.8%	37.7%

Table 5: Compiled Results for Calculated and Fixed z_{CHF} Models when Excluding Subcooled Film Boiling Points

Acknowledgments

This work was funded by the Reduced Gravity Cryogenic Transfer Project under the Cryogenic Fluid Management Portfolio Project under the Space Technology Mission Directorate at NASA.

Appendix A – Results for Calculated and Fixed z_{CHF} Runs

Case	Built-In Correlations MAPE	Built-In Correlations SMAPE	Built-In Correlations z_{CHF} % Error	Universal Correlations MAPE	Universal Correlations SMAPE	Universal Correlations z_{CHF} % Error
Run 127	107.1%	67.6%	12.8%	13.6%	18.3%	10.8%
Run 137	201.8%	81.0%	44.9%	102.0%	29.2%	10.4%
Run 140	251.6%	94.3%	57.7%	148.9%	42.2%	19.0%
Run 146	13.3%	14.0%	1.6%	44.1%	71.9%	31.5%
Run 147	16.5%	14.7%	1.6%	16.8%	17.2%	2.9%
Run 148	9.6%	10.0%	1.6%	18.8%	18.4%	2.5%
Run 149	14.5%	12.5%	1.6%	44.3%	38.8%	18.8%
Run 150	27.4%	23.3%	1.6%	26.4%	40.8%	18.7%
Run 158	13.4%	15.0%	1.6%	14.3%	13.6%	23.2%
Run 159	21.9%	19.5%	1.6%	42.3%	69.3%	30.0%
Run 160	27.9%	31.3%	1.6%	30.7%	50.4%	23.7%
Run 161	27.3%	32.8%	1.6%	45.0%	74.7%	28.9%
Run 162	17.8%	17.7%	1.6%	45.7%	80.4%	34.9%
Run 163	20.4%	20.3%	1.6%	14.3%	17.3%	26.2%
Run 164	23.8%	26.9%	1.6%	34.0%	55.7%	22.7%
Run 165	13.9%	15.2%	1.6%	13.5%	13.0%	24.1%
Run 166	16.0%	16.8%	1.6%	16.1%	14.2%	3.0%
Run 167	25.7%	27.0%	1.6%	34.4%	28.1%	2.7%
Run 168	46.9%	61.0%	1.6%	36.0%	42.4%	9.0%
Run 169	42.0%	48.3%	1.6%	76.5%	129.9%	54.2%
Run 170	37.9%	39.3%	1.6%	77.3%	132.0%	59.8%
Run 171	23.6%	24.4%	1.6%	38.6%	60.0%	22.6%
Run 172	13.1%	13.2%	1.6%	14.1%	13.2%	2.1%
Run 306	119.9%	41.3%	25.3%	18.9%	28.3%	4.6%
Run 311	223.9%	54.9%	25.3%	30.5%	43.7%	14.3%
Run 313	152.1%	43.9%	18.9%	48.2%	84.5%	38.0%
Run 317	196.3%	68.7%	31.8%	75.5%	35.6%	6.1%
Run 322	98.7%	33.0%	12.8%	33.6%	49.2%	15.6%
Mean	**47.2%**	**31.6%**	**7.4%**	**41.2%**	**46.9%**	**20.0%**

Table A-1: Lewis et al. 1962 [9] Hydrogen Calculated z_{CHF} Model Errors

	Nucleate Boiling			Film Boiling		
Run #	**# Datapoints**	**MAPE**	**SMAPE**	**# Datapoints**	**MAPE**	**SMAPE**
Run 127	2	5.3%	5.5%	11	25.0%	20.2%
Run 137	7	3.1%	3.1%	6	7.9%	7.8%
Run 140	8	6.3%	6.1%	5	7.4%	7.4%
Run 146	-	-	-	13	15.3%	17.1%
Run 147	-	-	-	13	17.2%	17.5%
Run 148	-	-	-	13	18.4%	16.3%
Run 149	-	-	-	7	26.4%	103.6%
Run 150	-	-	-	13	18.1%	15.0%
Run 158	-	-	-	13	10.4%	9.4%
Run 159	-	-	-	13	15.7%	15.4%
Run 160	-	-	-	13	30.5%	23.0%
Run 161	-	-	-	13	12.5%	12.3%
Run 162	-	-	-	13	22.1%	24.1%
Run 163	-	-	-	13	11.3%	10.9%
Run 164	-	-	-	13	20.9%	16.7%
Run 165	-	-	-	13	11.7%	10.0%
Run 166	-	-	-	13	16.8%	14.7%
Run 167	-	-	-	13	31.1%	23.8%
Run 168	-	-	-	13	35.4%	40.2%
Run 169	-	-	-	13	44.4%	44.8%
Run 170	-	-	-	13	27.9%	33.1%
Run 171	-	-	-	13	22.8%	17.7%
Run 172	-	-	-	13	14.5%	14.6%
Run 306	4	21.8%	24.6%	11	7.3%	7.6%
Run 311	4	35.2%	28.7%	11	8.1%	7.9%
Run 313	3	36.8%	28.9%	12	13.5%	12.5%
Run 317	5	28.1%	24.5%	10	15.1%	14.1%
Run 322	1	75.8%	54.9%	14	49.0%	32.3%
Mean	**34**	**16.5%**	**14.8%**	**334**	**18.9%**	**18.4%**

Table A-2: Lewis et al. 1962 [9] Hydrogen Fixed z_{CHF} Model Case Errors

Case	Built-In Correlations MAPE	Built-In Correlations SMAPE	Universal Correlations MAPE	Universal Correlations SMAPE
Run 1-1146	58.9%	84.7%	29.3%	34.7%
Run 3-1143	51.5%	71.6%	31.9%	39.7%
Run 2-1247	44.5%	59.1%	55.2%	80.9%
Run 4-1251	27.4%	33.2%	57.1%	69.8%
Run 1-542	32.3%	39.3%	39.3%	46.2%
Run 2-541	24.6%	26.5%	59.5%	65.2%
Run 6-201	32.7%	41.0%	47.2%	65.7%
Run 7-540	22.7%	25.2%	32.9%	47.0%
Run 9-204	37.4%	47.0%	25.4%	32.4%
Run 10-535	34.7%	43.7%	31.8%	41.2%
Run 11-536	42.7%	57.0%	31.3%	41.2%
Mean	**37.2%**	**48.0%**	**40.1%**	**51.3%**

Table A-3: Hendricks et al. 1966 [8] Hydrogen Calculated z_{CHF} Model Errors Including Subcooled Film Boiling Data

References

[1] M. Meyer, J. Hartwig, S. Sutherlin and A. Colozza, "Recent Concept Study for Cryogenic Fluid Management to Support Opposition Class Crewed Missions to Mars," Cryogenics, 129, 103622. 2023.

[2] J. Hartwig, A. Asensio and S. Darr, "Assessment of Existing Two Phase Heat Transfer Coefficient and Critical Heat Flux on Cryogenic Flow Boiling Quenching Experiments," International Journal of Heat and Mass Transfer, 93, 441 – 463. 2016.

[3] M. Mercado, N. Wong and J. Hartwig, "Assessment of Two-Phase Heat Transfer Coefficient and Critical Heat Flux Correlations for Cryogenic Flow Boiling in Pipe Heating Experiments," International Journal of Heat and Mass Transfer, 133, 295-315. 2019.

[4] V. Ganesan, R. Patel, J. Hartwig and I. Mudawar, "Review of Databases and Correlations for Saturated Flow Boiling Heat Transfer Coefficient for Cryogens in Uniformly Heated Tubes, and Development of New Consolidated Database and Universal Correlations," International Journal of Heat and Mass Transfer, 179, 121656. 2021.

[5] V. Ganesan, R. Patel, J. Hartwig and I. Mudawar, "Universal Critical Heat Flux (CHF) Correlations for Cryogenic Flow Boiling in Uniformly Heated Tubes," International Journal of Heat and Mass Transfer 166, 120678. 2021.

[6] V. Ganesan, R. Patel, J. Hartwig and I. Mudawar, "Universal Correlations for Post-CHF Saturated and Superheated Flow Film Boiling Heat Transfer Coefficient, Minimum Heat Flux and Rewet Temperature for Cryogenic Fluids in Uniformly Heated Tubes," International Journal of Heat and Mass Transfer 195, 123054. 2022.

[7] V. Ganesan "Development of Universal Databases and Predictive Tools for Two-Phase Heat Transfer and Pressure Drop in Cryogenic Flow Boiling Heated Tube Experiments" Dissertation, Purdue University, August, 2023.

[8] R.C. Hendricks, R.W. Graham, Y.Y. Hsu, and R. Friedman, "Experimental Heat-Transfer Results for Cryogenic Hydrogen Flowing in Tubes at Subcritical and Supercritical Pressures to 800 Pounds per Square Inch Absolute," NASA Technical Note D-3095, 1966.

[9] J.P. Lewis, J.H. Goodykoontz, and J.F. Kline, "Boiling Heat Transfer to Liquid Hydrogen and Nitrogen in Forced Flow," NASA Technical Note, D-1314, 1962.

[10] J.W. Hartwig, H. Hu, J. Styborski, and J.N. Chung, "Comparison of Cryogenic Flow Boiling in Liquid Nitrogen and Liquid Hydrogen," International Journal of Heat and Mass Transfer 88, 662 – 673. 2015.

[11] M. Shah, "Unified Correlation for Heat Transfer during Boiling in Plain Mini/Micro and Conventional Channels," International Journal of Refrigeration 74, 606–626. 2017.

[12] O. Kartuzova and M. Kassemi, "Modeling K-Site LH_2 Tank Chilldown and No Vent Fill in Normal Gravity," AIAA Paper 2017-4662, July 2017.

[13] M. Baldwin, V. Ganesan, J.W. Hartwig, A. LeClair, A. Majumdar, and I. Mudawar, "Modeling of Cryogenic Heated-Tube Flow Boiling Experiments of Nitrogen and Methane with the Generalized Fluid System Simulation Program," *Advances in Cryogenic Engineering* 2024.

[14] A. LeClair, M. Baldwin, A. Majumdar, J.W. Hartwig, V. Ganesan, and I. Mudawar, "Modeling of Cryogenic Heated-Tube Boiling Experiments of Hydrogen and Helium with the Generalized Fluid System Simulation Program," *Cryogenics* 2024.

[15] E. Tesny, J.W. Hartwig, V. Ganesan, I. Mudawar, and M. Mercado, "Validation of Universal Cryogenic Flow Boiling Correlations in Thermal Desktop for Liquid Helium," *Advances in Cryogenic Engineering* 2024.

[16] M. Mercado, E. Tesny, J.W. Hartwig, V. Ganesan, and I. Mudawar, "Validation of Universal Cryogenic Flow Boiling Correlations in Thermal Desktop for Liquid Methane and Liquid Nitrogen," *Cryogenics* 2024.

[17] C&R Technologies, "TD Suite Manual for Thermal Desktop, TD Direct, and SINDA/FLUINT. Version 6.3, Thermal Desktop Patch 13, SINDA/FLUINT Patch 10," C&R Technologies, 2022.

[18] J.C. Chen, "Correlation for Boiling Heat Transfer to Saturated Fluids in Convective Flow," Industrial & Engineering Chemistry Process Design and Development 5, 322 – 329. 1966.

[19] F.W. Dittus and L.M.K. Boelter, "Heat Transfer in Automobile Radiators of the Tubular Type," International Communications in Heat and Mass Transfer 12, 3 – 22. 1985.

[20] N. Zuber, "On the Stability of Boiling Heat Transfer," Transactions of the Americal Society of Mechanical Engineers 80, 711 - 720 1958.

[21] W.R. Gambill, "Generalized Prediction of Burnout Heat Flux for Flowing, Subcooled, Wetting Liquids," *Chemical Engineering Progress Symposium* 59, 71 – 87. 1963.

[22] J. Ramilson, and J. Lienhard, "Transition Boiling Heat Transfer and the Film Transition Regime," Journal of Heat and Mass Transfer, vol. 109, 1987.

[23] J. Bromley, N. LeRoy, and J. Robbers, "Heat Transfer in Forced Convection Film Boiling," Industrial and Engineering Chemistry, p. 2639, 1953.
[24] J.E. Leonard et al., “Low-Flow Film Boiling Heat Transfer on Vertical Surfaces, Part 2 Empirical Formulations and Application to BWR-LOCAD Analysis,” Solar and Nuclear Heat Transfer, AIChE Symposium Series, No 164, Vol 73, 1977. Corrected using J.G. Andersen, “Low-Flow Film Boiling Heat Transfer on Vertical Surfaces, Part 1 Theoretical Model,” Solar and Nuclear Heat Transfer, AIChE Symposium Series, No 164, Vol 73, 1977.
[25] D. Groeneveld and C. Snoek, "A Comprehensive Examination of Heat Transfer Correlations Suitable for Reactor Safety Analysis," Multiphase Science and Technology, 1986.
[26] J. Lewis, J. Goodykoontz, and J. Kline, "Boiling Heat Transfer to Liquid Hydrogen and Nitrogen in Forced Flow," 1962.
[27] J. Hartwig, V. Ganesan, A. Johnson, I. Mudawar, A. Leclair, E. Tesny, M. Baldwin, A. Majumdar and M. Mercado, "A Continuous Flow Boiling Curve in the Heating Configuration Based on New Cryogenic Universal Correlations," International Journal of Heat and Mass Transfer, 2024.